Holmberg, Nico; Laasonen, Kari

Diabatic model for electrochemical hydrogen evolution based on constrained DFT configuration interaction

Published in:
Journal of Chemical Physics

DOI:
10.1063/1.5038959

Published: 11/09/2018

Document Version
Peer-reviewed accepted author manuscript, also known as Final accepted manuscript or Post-print

Please cite the original version:
Holmberg, N., & Laasonen, K. (2018). Diabatic model for electrochemical hydrogen evolution based on constrained DFT configuration interaction. *Journal of Chemical Physics*, *149*(10), Article 104702. https://doi.org/10.1063/1.5038959

Diabatic model for electrochemical hydrogen evolution based on constrained DFT configuration interaction

Nico Holmberg[1] and Kari Laasonen[1, a)]

Department of Chemistry and Materials Science, Aalto University, P.O. Box 16100, 00076 Aalto, Finland

(Dated: 13 July 2018)

The accuracy of density functional theory (DFT) based kinetic models for electrocatalysis is diminished by spurious electron delocalization effects, which manifest as uncertainties in the predicted values of reaction and activation energies. In this work, we present a constrained DFT approach to alleviate overdelocalization effects in the Volmer-Heyrovsky mechanism of the hydrogen evolution reaction (HER). This method is applied a posteriori to configurations sampled along a reaction path to correct their relative stabilities. Concretely, the first step of this approach involves describing the reaction in terms of a set of diabatic states that are constructed by imposing suitable density constraints on the system. Refined reaction energy profiles are then recovered by performing a configuration interaction (CDFT-CI) calculation within the basis spanned by the diabatic states. After a careful validation of the proposed method, we examined HER catalysis on open-ended carbon nanotubes and discovered that CDFT-CI increased activation energies and decreased reaction energies relative to DFT predictions. We believe that a similar approach could also be adopted to treat overdelocalization effects in other electrocatalytic proton-coupled electron transfer reactions, e.g., in the oxygen reduction reaction.

PACS numbers: 82.45.Jn, 82.20.Wt, 82.20.Gk, 31.15.em

---

a) Corresponding author: kari.laasonen@aalto.fi

I. INTRODUCTION

Two prevalent paradigms steer the development of new catalyst materials in the field of computational electrochemistry.[1–3] The first involves relating experimentally measured catalytic activities of well-defined materials to a reduced set of simple and easily calculable descriptive variables, such as the adsorption (free) energies of reaction intermediaries.[4–6] New catalyst candidates can subsequently be screened from a large group of materials by computing the values of the descriptive variables. The approach taken in the second paradigm is totally opposite, where the ultimate goal is the development of an accurate kinetic model of the catalytic process that mimics experimental reaction conditions as closely as possible.[7–10] While both of these methods can be considered as complementary approaches, they suffer from their own limitations and typically only one of them is adopted depending on the specific application. Nevertheless, recent efforts[3,11] have begun blurring the boundary between these approaches, and the advance towards a more unified treatment is likely to accelerate in the future through the broader utilization of machine learning methods.[12–14]

One of the strengths of the kinetic modeling approach is that it attempts to address phenomena that are extremely difficult to resolve based on experiments alone owing to resolution limitations. As an example of such an application, the method has elucidated the effects of different surface functionalizations on the electrocatalytic activity of carbon nanotubes (CNTs) and other carbon-based materials towards the hydrogen evolution reaction (HER), $2H^+ + 2e^- \rightarrow H_2$.[15]

The technological relevance and the relative simplicity of HER have made the reaction a vital proving ground for testing new catalyst models and assessing their accuracy. Density functional theory (DFT) based simulations are at the core of these HER models, and resolving the inherent deficiencies of DFT is an integral part on the path towards better catalyst models. In addition to issues related to the accurate description of the electrode-electrolyte interface,[16–18] one major issue that affects the quality of DFT simulations is the choice of the exchange-correlation functional. Specifically, commonly used functionals are prone to errors resulting from spurious electron delocalization effects, which are ultimately caused by self-interaction error.[19] This leads to uncertainty in the predicted values of reaction and activation energies, which are the key quantities needed in the construction of reaction energy diagrams – the cornerstones for gauging catalyst performance from simulations.

In this work, we propose a constrained DFT (CDFT)[20–22] model for alleviating the effects of spurious electron delocalization in the Volmer-Heyrovsky mechanism of HER, which is comprised of the following two proton-coupled electron transfer (PCET) reactions

$$\begin{aligned} \mathrm{H}^+ + \mathrm{e}^- &\rightarrow \mathrm{H}^* \quad \text{(Volmer)} \\ \mathrm{H}^+ + \mathrm{H}^* + \mathrm{e}^- &\rightarrow \mathrm{H}_2 \quad \text{(Heyrovsky)} \end{aligned} \tag{1}$$

where H^* denotes a surface adsorbed hydrogen. The first step of this model involves representing the reaction in terms of a set of diabatic, charge localized electronic states that are created by enforcing suitable charge and magnetization density constraints on the system. The choice of which diabatic electronic states to include in the model is motivated by adapting the Soudackov–Hammes-Schiffer[23–25] (SHS) theory for concerted PCET reactions. Subsequently, these CDFT diabatic states are used as the basis for a configuration interaction (CDFT-CI) calculation in order to recover adiabatic potential energy profiles for the Volmer-Heyrovsky reaction. Van Voorhis and coworkers[26] originally developed a similar CDFT-CI approach to treat static correlation, which they later successfully applied to improve the predictions of activation energies for simple gas phase chemical reactions.[27] Although there are other methods for mitigating the effects of charge overdelocalization, the method we propose in this work is relatively cheap to apply as an a posteriori correction to existing DFT reaction calculations, and the explicit generation of the diabatic electronic states provides grounds for additional analysis.

The remainder of this paper is structured as follows. First, we will establish the theoretical basis for using the CDFT-CI model by discussing the SHS theory and its extension to the Volmer-Heyrovsky reaction in Sec. II A. The algorithms that were implemented to construct the diabatic CDFT states and to perform configuration interaction simulations are then detailed in Sec. II B. Sec. III summarizes the computational methods used in the present study. Benchmark calculations are carried out in Section IV A using a simple model system to validate the proposed CDFT-CI method. Subsequently in Secs. IV B-IV C, we apply the method to a more complex open-ended carbon nanotube based catalyst, originally studied in Ref. 28, and compare the predictions of standard DFT and CDFT-CI for key catalytic performance indicators. The causes for observed differences in DFT and CDFT-CI potential energy surfaces are elaborated in Sec. IV D based on results from earlier sections. A critical analysis on the effects of the CDFT-CI active space size will also be presented. The main conclusions of this study are summarized in Sec. V.

II. THEORY

To reiterate, our goal is to establish a theoretical foundation for modeling the elementary steps of HER with constrained DFT based configuration interaction in an effort to mitigate the effects of spurious electron delocalization, which causes uncertainty in the values of HER reaction and activation energies. The Soudackov–Hammes-Schiffer theory[23–25] for concerted PCET reactions, formulated in a more general setting with distinct proton/electron donor and acceptor groups, provides the necessary tools for this task. Consequently, in Section II A, we will first describe the main aspects of the SHS model before adapting it to the Volmer-Heyrovsky reaction. The algorithms for performing CDFT-CI simulations are then detailed in Section II B.

A. SHS model applied to electrocatalytic HER

The SHS model[23–25] for PCET reactions uses an analogous theoretical framework to Marcus theory of electron transfer (ET, see e.g. Ref. 29 for a recent review), which provides a fruitful basis for describing the model. The model can be considered completely general in the sense that it can treat both sequential and concerted electron-proton transfer reactions as well as the special case of hydrogen atom transfer (HT), where an electron and a proton are transferred between the same donor and acceptor groups, and the reaction does not involve significant redistribution of charge. The relation between Marcus, SHS, and other related theories has previously been explored in depth in the excellent review article by Migliore et al.,[30] which also includes a comprehensive treatise of the theoretical concepts involved in PCET reactions. We will therefore keep our treatment concise.

To establish a connection between Marcus theory and the SHS model, consider the following generic proton-coupled electron transfer reaction involving the transfer of one proton and one electron

$$\mathrm{D_e^-{-}D_p{-}H^+ + A_p{-}A_e \rightarrow D_e{-}D_p + H^+{-}A_p{-}A_e^-} \tag{2}$$

where D_e, A_e are the electron and D_p, A_p the proton donating and accepting groups, respectively. The direction for proton and electron transfer is assumed to be the same without loss of generality. If this reaction featured only electron transfer, then according to Marcus theory, it could be described as a transition between two charge localized diabatic electronic states, which represent the initial and final states of the reaction (the term 'nonadiabatic' is used interchangeably in some publications), with solvent reorganization acting as the driving force of the reaction.[29] Analogous to the case of ET, the SHS model associates four diabatic electronic states with the PCET reaction as depicted in Fig. 1a.[23] The diagonal pathway in Fig. 1a corresponds to the net concerted PCET reaction with no stable intermediate states, whereas the pathways along the sides of the square represent sequential mechanisms where proton transfer (PT) either proceeds or follows the electron transfer step. The relative energies of the diabatic states and the couplings between them determine the actual reaction mechanism.

The transferring proton is treated as an additional inner-sphere solute mode to the electronic subsystem and collective solvent coordinates are associated with both modes.[23] The quantum mechanical character of the proton is included explicitly in the model by replacing the purely electronic states used in Marcus theory with mixed electron-proton vibronic states

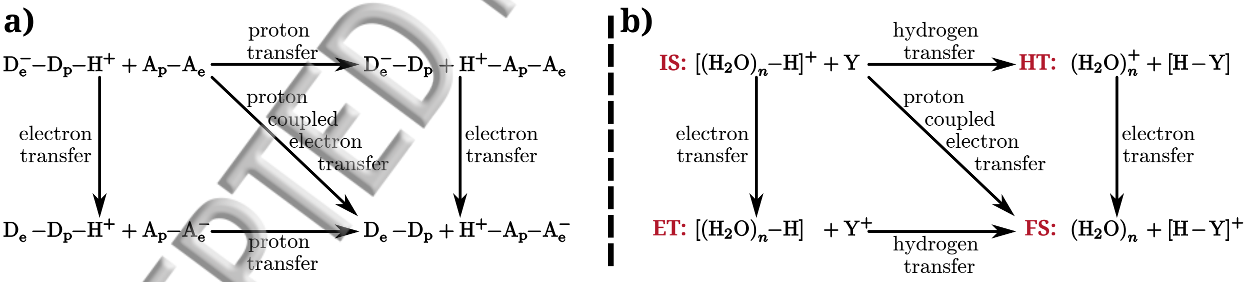

FIG. 1. a) The four diabatic electronic states considered in the SHS model for PCET.[23] The diagonal pathway represents the concerted reaction, whereas the off-diagonal pathways correspond to sequential ET/PT and PT/ET mechanisms. b) Extension of the SHS model to the Volmer reaction, the initial step of the electrochemical hydrogen evolution reaction. The proton transfer steps from a) are replaced by hydrogen atom transfer steps. The diabatic states involved in the reaction are denoted by the red labels. The depicted charge states apply to systems with a net unit positive charge. If the system is charge neutral, the charges of all Y containing fragments must be decreased by one.

$|\Psi^{I}_{\mu}\rangle$. The vibronic wavefunctions can be expressed as the product of a diabatic electronic component $|\psi^{I}\rangle$ and the proton vibrational wavefunction $|\chi_{\mu}\rangle$, or more generally, as the linear combination of such products.[31] The proton vibrational wavefunction can be evaluated by discretizing the motion of the proton onto a grid that spans the appropriate reaction coordinate, and by solving the nuclear Schrödinger equation in the potential energy field generated by the electrons.[32–34]

In the basis of the vibronic wavefunctions, the PCET reaction is modeled as a diabatic transition between initial (IS) and final state (FS) wavefunctions $|\Psi^{\mathrm{IS}}_{\mu}\rangle \rightarrow |\Psi^{\mathrm{FS}}_{\nu}\rangle$, where the off-diagonal states from Fig. 1a are either ignored if they lie far above the diagonal states, or they can be combined with the diagonal states into effective states using block diagonalization (see Section II B).[25] Assuming that the vibronic coupling between the states is small, $V_{\mu\nu} = \langle\Psi^{\mathrm{IS}}_{\mu}|\mathcal{H}|\Psi^{\mathrm{FS}}_{\nu}\rangle \ll k_{B}T$, and that other conditions[35] of the Fermi golden rule limit hold, the rate of a vibronically diabatic PCET reaction can be expressed in a form that closely parallels the Marcus ET rate equation.[29] Concretely, the rate constant for a diabatic PCET reaction at fixed proton acceptor-donor separation is given by[36]

$$k = \sum_{\mu} P_{\mu} \sum_{\nu} \frac{|V_{\mu\nu}|^{2}}{\hbar} \sqrt{\frac{\pi}{\sigma_{\mu\nu} k_{\mathrm{B}} T}} \exp\left[-\frac{(\Delta G^{\circ}_{\mu\nu} + \sigma_{\mu\nu})^{2}}{4\sigma_{\mu\nu} k_{\mathrm{B}} T}\right] \tag{3}$$

where the summations μ and ν are over the reactant and product vibrational states, respectively, P_{μ} is the Boltzmann probability of observing the vibrational state μ, $\sigma_{\mu\nu}$ is the solvent reorganization energy, and $\Delta G^{\circ}_{\mu\nu}$ is the reaction free energy. The form of the vibronic coupling $V_{\mu\nu}$ depends on the degree of electron-proton adiabacity and it can be gauged e.g. using the semiclassical diagnostic $p = \tau_{\mathrm{p}}/\tau_{\mathrm{e}}$, which relates the rates of proton tunneling and electronic transition.[25,37] In the electronically diabatic limit, $p \ll 1 \Leftrightarrow \tau_{\mathrm{e}} \gg \tau_{\mathrm{p}}$, the electrons are unable to rearrange fast enough for the proton to stay on the ground electronic state, and the vibronic coupling is given by the product of the electronic coupling and the vibrational overlap $V^{\mathrm{diabatic}}_{\mu\nu} = V^{\mathrm{el}} \langle\chi_{\mu}|\chi_{\nu}\rangle$. In the opposite limit, $p \gg 1$, electrons respond instantly to proton motion and the PCET reaction can be fully characterized by the ground adiabatic electronic state.

Having summarized the main aspects of the SHS model, we are now ready to apply the model to the electrochemical hydrogen evolution reaction proceeding via the Volmer-Heyrovsky mechanism. The former reaction step will be primary focus of this paper. An extension of the model to the Heyrovsky reaction will be briefly covered in Section IV C. In order to make the connection to the SHS model explicit, we rewrite the Volmer reaction from Eq. (1) as follows

$$[(\mathrm{H_2O})_n\!-\!\mathrm{H}]^+ + \mathrm{Y} \rightarrow (\mathrm{H_2O})_n + [\mathrm{H}\!-\!\mathrm{Y}]^+ \qquad (4)$$

where n is a positive integer whose value depends on how the solvated proton is modeled, e.g., $n = 1$ for the hydronium and $n = 2$ for the Zundel cation, respectively, and Y is the electron donating catalyst surface. We would like to emphasize that the value of n includes only those water molecules that actively participate in the reaction; the system may well contain additional 'bystander' molecules for modeling hydration effects. Comparison of Eqs. (2) and (4) shows that the only difference between the reactions is the apparent lack of electron transfer in the Volmer reaction. This is due to the fact that the proton is reduced to a hydrogen atom in the reaction: as the proton traverses the reaction coordinate, the proton accepts an electron from the donor surface Y and simultaneously forms a covalent bond with the surface. Consequently, the excess positive charge that is initially (mostly) located on the proton becomes fully delocalized over the reaction product $\mathrm{H} - \mathrm{Y}$ in the final state. We have emphasized this charge delocalization by using square brackets in Eq. (4).

Fig. 1b shows the four diabatic electronic states that can be associated with the Volmer reaction. The states on the diagonal are analogous to the SHS model and represent the reactant (IS) and product (FS) states of the reaction, where both the electron and proton are either localized on the donor or acceptor species. Continuing with the connection to the SHS model, we may identify the ET diabat as a state where the donor Y has already reduced the proton to a hydrogen but the atom still remains (loosely) associated with the proton donor $(\mathrm{H_2O})_n$. To complete the sequential reaction pathway IS → ET → FS, the final step now involves a hydrogen atom transfer step in contrast to the SHS model where proton transfer was the concluding step. The last diabatic state, labeled HT, represents the intermediary configuration of the opposite sequential HT/ET mechanism. It is worth noting that the state associated with proton transfer in the SHS model, Fig. 1a, is fully equivalent with the reactant (IS) state in the Volmer model due to the CDFT methodology used in creating the diabatic states (vide infra).

At first glance, the off-diagonal states in Fig. 1b, especially the HT state, appear somewhat artificial because the existence of the required intermediate configurations is improbable in electrocatalytic hydrogen evolution. Glancing forward to Sections IV A-IV C, these states will indeed be high energy states compared to the reactant and product states. However, the off-diagonal diabats should not be interpreted as true observable states. They are primarily included for completeness in the active space of the CDFT configuration interaction calculation, and as subsequent Sections will show, the states will mainly play a small role in the transition state region. First, however, we shall address how to reliably generate the diabatic electronic states defined in Fig. 1b, which will be the key step controlling the accuracy of the Volmer model.

B. Configuration interaction based on constrained DFT

As shown in the previous section, applying the SHS model to describe the elementary steps of HER requires both the adiabatic and diabatic electronic states associated with the reaction. The necessary diabatic states could, in principle, be obtained from the adiabatic wavefunction with localization techniques.[38] However, since HER catalyst models typically require the use of large systems due to their complexity (see e.g. Ref. 7), only GGA level DFT calculations of such systems are routinely tractable with current computational resources, which are known to suffer from spurious electron delocalization due to self-interaction error.[19] In an effort to mitigate these errors, we have opted for an alternative approach where the diabatic states are first explicitly constructed by means of constrained DFT, and the adiabatic electronic states are subsequently calculated from the diabatic states using configuration interaction. The theoretical foundations of CDFT[20–22] and CDFT-CI[26,27] have been discussed extensively in the literature. Here, we will present only the main attributes of the algorithm that we have implemented to perform CDFT-CI simulations of HER in solvated environments, as an extension of our earlier implementation[39] which was limited to systems with a single constraint and two diabatic states.

In CDFT, a diabatic electronic state is constructed by supplementing the standard Kohn-Sham energy expression with suitable external potentials in an extended Lagrangian approach. The role of these constraint potentials is to enforce the desired charge and spin localization conditions in atom centered regions of the system. Assuming M arbitrary density constraints, the CDFT energy functional can be written as the dual optimization problem[22]

$$E^{\mathrm{CDFT}}[\rho(\boldsymbol{r}),\boldsymbol{\xi}] = \max_{\boldsymbol{\xi}} \min_{\rho(\boldsymbol{r})} \left(E^{\mathrm{KS}}[\rho(\boldsymbol{r})] + \sum_{c}^{M} \xi_c \left[\sum_{i=\uparrow,\downarrow} \int w_c^i(\boldsymbol{r}) \rho^i(\boldsymbol{r}) \mathrm{d}\boldsymbol{r} - N_c \right] \right) \tag{5}$$

where $\boldsymbol{\xi}$ are the Lagrange multipliers associated with the constraints, $w_c^i(\boldsymbol{r})$ is an atom centered real space weight function that enforces the constraint by operating on the density, and N_c is the constraint target value. The conventions $w_c^\uparrow = w_c^\downarrow = w_c$ and $w_c^\uparrow = -w_c^\downarrow = w_c$ are adopted to treat total $(\rho^\uparrow + \rho^\downarrow)$ and magnetization $(\rho^\uparrow - \rho^\downarrow)$ density constraints, respectively. The Becke[40] population analysis method with atomic size adjustments has been selected as the weight function w_c in the present CDFT implementation. A detailed description of the properties and efficient construction of the Becke weight function is given in our earlier publication.[39]

The constraint target value, N_c, is a measure of the desired number of electrons per molecular group in each of the diabatic electronic states. Because the formal number of electrons per molecule is poorly defined when molecules interact strongly,[27,41] we employ so called fragment based constraints to define the constraint target values. This process involves first splitting the full system into two isolated fragments, $\mathrm{I} = \{\mathrm{A}, \mathrm{B}\}$, depending on the modeled diabatic state. For example, to simulate the state labeled IS in Fig 1b, the system would be split into the fragments $[(\mathrm{H_2O})_n\text{–}\mathrm{H}]^+$ and Y. The spin densities, $\widetilde{\rho}_{\mathrm{I}}^i$, of these isolated fragments are then separately optimized and saved to disk. Subsequently, the constraint target values in the true interacting system are computed from the isolated densities according to

$$\widetilde{N}_c = \sum_{i=\uparrow,\downarrow} \int w_c^i(\boldsymbol{r}) (\widetilde{\rho}_{\mathrm{A}}^i(\boldsymbol{r}) + \widetilde{\rho}_{\mathrm{B}}^i(\boldsymbol{r})) \mathrm{d}\boldsymbol{r} \tag{6}$$

A number of remarks are in order to further elucidate the fragment constraint approach. Although for notational convenience the active proton and electron are associated with the donor or acceptor fragments in Fig. 1b, we wish to emphasize that the fragment constraint formalism imposes no actual chemical bonds between the components. Instead, the CDFT constraint target values for each diabat are fully determined by the superposition of the reference fragment densities $\widetilde{\rho}_{\mathrm{I}}^i$ through Eq. (6), which in turn are the self-consistent DFT minimum energy densities of the isolated fragments with a selected exchange-correlation functional. Three consequences follow directly from the use of the fragment constraints.

Firstly, the partial charges of the reacting proton and other components of the system will in general be fractional in contrast to the simplified picture depicted in Fig. 1b. Secondly, the CDFT target values and hence the partial charges are not fixed quantities but will vary along the reaction coordinate. Finally, as the system transitions from diabatic state to another, the partial charges will exhibit non-integer changes which slightly obfuscate the interpretation of the different CDFT diabats. These distinctions are especially important in the transition state region – a matter we will discuss in more depth in Section IV D.

The optimization problem defined by Eq. (5) can be solved iteratively using a two tiered self-consistent field (SCF) approach of alternating energy minimizations along $\rho(\boldsymbol{r})$ and maximizations along $\boldsymbol{\xi}$. Standard SCF algorithms can be employed for the inner loop energy minimization with a fixed value of $\boldsymbol{\xi}$.[42] To derive an algorithm for the outer energy maximization along $\boldsymbol{\xi}$, observe that the exact solution satisfies the following identity

$$\boldsymbol{c}(\boldsymbol{\xi}) = \left[\sum_{i=\uparrow,\downarrow} \int w_1^i(\mathbf{r})\rho^i(\mathbf{r})d\mathbf{r} - N_1, \quad \cdots \right]^{\mathrm{T}} = \mathbf{0} \tag{7}$$

In the above expression, the function $\boldsymbol{c}$ depends on $\boldsymbol{\xi}$ parametrically: for any fixed value of $\boldsymbol{\xi}$, the inner loop minimization of the Kohn-Sham energy produces a unique density $\rho(\boldsymbol{r})$ and hence a new value of $\boldsymbol{c}$. According to Eq. (7), the outer loop energy maximization can be viewed as a root finding problem that can be terminated when a value of $\boldsymbol{\xi}$ is found that satisfies $\max|\boldsymbol{c}(\boldsymbol{\xi})| \leq \varepsilon$ at some fixed convergence threshold ε. O'Regan and Teobaldi[43] have analyzed the necessary conditions to guarantee the uniqueness of this solution. The Newton-Raphson method can be applied to iteratively solve the root finding problem by generating a new guess for $\boldsymbol{\xi}_n$ at step n according to

$$\boldsymbol{\xi}_n = \boldsymbol{\xi}_{n-1} - \alpha \mathbf{J}_n^{-1} \boldsymbol{c}(\boldsymbol{\xi}_{n-1}) \tag{8}$$

where $\alpha > 0$ is a step size, whose magnitude is optimized with backtracking line search, and $\mathbf{J}^{-1}$ is the inverse of the Jacobian matrix. The elements of the Jacobian matrix are approximated with finite differences, e.g., using a first order forward difference stencil

$$\mathbf{J}_{i,j} = \frac{\partial c_i}{\partial \xi_j} \approx \frac{c_i(\boldsymbol{\xi} + \boldsymbol{\delta}_j) - c_i(\boldsymbol{\xi})}{|\boldsymbol{\delta}_j|} \tag{9}$$

where $\boldsymbol{\delta}_j$ is a small perturbation of the jth component of $\boldsymbol{\xi}$. The computational cost of calculating the Jacobian matrix amounts to a sizable fraction of the total cost of the

CDFT method when multiple constraints are imposed on the system. Different strategies can be adopted to mitigate the computational cost: the same Jacobian matrix can be reused for multiple iterations, or the matrix can be iteratively updated after the first step by leveraging a quasi-Newton method, such as Broyden's method. These strategies are, however, unnecessary in the current context where the diabatic electronic states defined in Fig. 1b are solved for a discrete set of atomic configurations translated continuously along a reaction coordinate. With the exception of the first atomic configuration, the CDFT energy optimization of any subsequent configurations can be restarted from the converged solution of the previous configuration, which results in a significant reduction in the number of required iterations with respect to $\boldsymbol{\xi}$, see Section III for further details.

Configuration interaction can be employed to recover the adiabatic energy surfaces and corresponding Slater determinants, $|\Phi\rangle$, from a set of diabatic CDFT states $\{|\Phi_i^{\mathrm{CDFT}}\rangle\}_i$.[26] Specifically, the adiabatic state is expanded in the basis of the constrained states

$$|\Phi\rangle = \sum_i c_i \left|\Phi_i^{\mathrm{CDFT}}\right\rangle, \sum_i c_i^2 = 1 \tag{10}$$

Here, the squares of the expansion coefficients, c_i^2, can be interpreted as the weight each CDFT state contributes to the adiabatic state $|\Phi\rangle$. The adiabatic states and their energies are obtained by solving the generalized eigenvalue equation

$$\mathbf{HC} = \mathbf{SC\Lambda} \tag{11}$$

where $\mathbf{H}$ is the effective Hamiltonian matrix with elements $\mathbf{H}_{i,j} = \langle\Phi_i^{\mathrm{CDFT}}|\mathcal{H}_{\mathrm{KS}}|\Phi_j^{\mathrm{CDFT}}\rangle$, $\mathcal{H}_{\mathrm{KS}}$ is the Kohn-Sham Hamiltonian, $\mathbf{C}$ is the matrix of expansion coefficients, $\boldsymbol{\Lambda} = \mathrm{diag}(\lambda_i)$ contains the eigenvalues λ_i of $\mathbf{H}$, and $\mathbf{S}$ is the overlap matrix comprised of terms $\mathbf{S}_{i,j} = \langle\Phi_i^{\mathrm{CDFT}}|\Phi_j^{\mathrm{CDFT}}\rangle$. The diagonal of $\mathbf{H}$ contains the energies of the diabatic CDFT states, whereas the off-diagonal elements are calculated according Eq. (12) to ensure $\mathbf{H}$ is symmetric.[22]

$$\mathbf{H}_{i,j} = \mathbf{H}_{j,i} = \frac{E_i^{\mathrm{CDFT}} + E_j^{\mathrm{CDFT}}}{2}\mathbf{S}_{i,j} - \sum_c \left\langle \Phi_i^{\mathrm{CDFT}} \left| \frac{\xi_c^i w_c^i(\boldsymbol{r}) + \xi_c^j w_c^j(\boldsymbol{r})}{2} \right| \Phi_j^{\mathrm{CDFT}} \right\rangle \tag{12}$$

We will conclude this section by summarizing the main steps of the proposed strategy for applying CDFT-CI to model the electrochemical hydrogen evolution reaction on the basis of the SHS model. First, the reaction is discretized into a set of configurations along the reaction coordinate. For each atomic configuration, the necessary isolated fragment densities are then optimized and used as input in CDFT simulations for solving the diabatic electronic states defined in Fig. 1b. Finally, the adiabatic energy profile along the reaction coordinate can be constructed by performing CDFT-CI multireference calculations on the set of obtained diabatic states. In general, the full set of four diabatic states should be included in the CDFT-CI calculation for accuracy reasons. However, because the SHS model is a two state model, the number of diabatic states must be reduced in order to compute other quantities defined in the SHS model, e.g., the semiclassical adiabacity parameter p.[25,37] This can be achieved by completely ignoring the ET and HT diabatic states, which are as noted before higher in energy than the IS and FS states, or by combining the (IS, ET) and (FS, HT) pairs into two effective diabatic states that describe the reactant and product states using block diagonalization. The block diagonalization process has been illustrated in Fig. 2. The effects of using different sets of diabatic states in CDFT-CI will be explored in detail in Section IV.

The block diagonalization process is also advantageous for including the effects of explicit solvation in the model. Explicit solvation has typically been considered in reaction path simulations of HER due to the importance of hydrogen bonding. At the same time, explicit

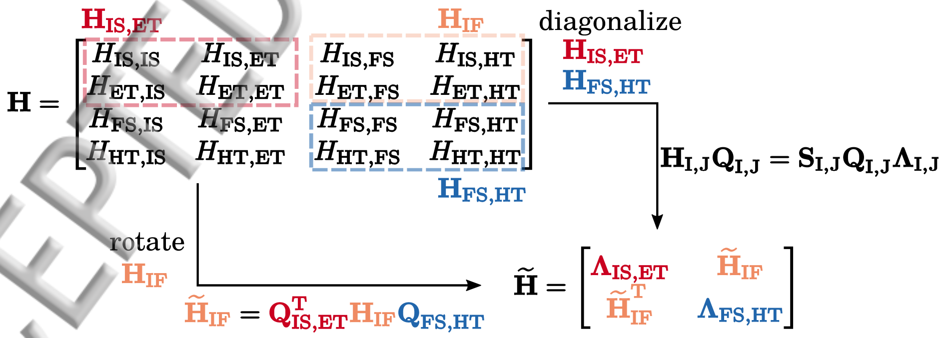

FIG. 2. Block diagonalization of the effective CDFT-CI Hamiltonian matrix $\mathbf{H}$. The diabatic states involved in the reaction are shown in Fig. 1b and the couplings between them are computed with Eq. (12). The diagonal blocks ($\mathbf{H}_{\mathrm{IS,ET}}, \mathbf{H}_{\mathrm{FS,HT}}$) are diagonalized yielding eigenvectors that are used to rotate the off-diagonal block $\mathbf{H}_{\mathrm{IF}}$. In practice, only the lowest energy eigenvalues and eigenvectors of the diagonal blocks are retained, reducing the rank of the resulting matrix $\widetilde{\mathbf{H}}$ in half.

solvation is problematic to include in fragment based CDFT constraints because only one of the fragments can be solvated, causing any solvation effects associated with the opposing choice to be fully ignored. Moreover, there is no clear reason to favor solvating one fragment over the other which leads to a degree of ambiguity in the model. This issue can be avoided altogether by taking advantage of block diagonalization during CDFT-CI, since the diabatic CDFT states for both solvation cases can be modeled and combined into one effective state with the method. The permutation where neither state is solvated, which would require a total of three fragments instead of two, has been ignored throughout this paper.

III. COMPUTATIONAL METHODS

The CDFT-CI method described in Section II B has been implemented in a development version of the open source quantum chemistry software CP2K.[44,45] We validated our implementation by reproducing some of the results of Hammes-Schiffer et al.[46–48] for the PCET self-exchange reaction in the phenoxyl-phenol system. The exact details and results of these simulations are presented in the Supplementary Material.

To confirm that the model introduced in Sec. II A is applicable to the study of eletrocatalytic hydrogen evolution, extensive benchmark calculations were carried out for the Volmer reaction in a system containing a hexa-peri-hexabenzocoronene $C_{42}H_{18}$ (HBC, see Fig. S2 in the Supplementary Material) molecule as a model catalyst. The impact of using different proton donors (hydronium H_3O^+ vs Zundel $H_5O_2{}^+$cation) and the choice of which diabatic electronic states to include in the CDFT-CI calculation were investigated in these simulations. The proposed block diagonalization strategy for considering explicit solvation effects in the reaction model was also tested. The main results of this manuscript are subsequently obtained by applying the model to HER catalysis in solvated open-ended carbon nanotube systems with a Zundel proton donor, which have been originally studied in Ref. 28. Concretely, we gauge how key catalytic performance indicators, i.e., the reaction and activation energies, are affected when standard DFT methods are contrasted with the developed CDFT-CI model. The examined surface sites and hydrogen coverage conditions have been detailed in Table S3 in the Supplementary Material. Explicit solvent molecules are included in both systems with a droplet model, as depicted in Fig. S2 in the Supplementary Material for HBC.

For the benchmark simulations, the axis connecting one of the central six ring carbon atoms and the proton donor oxygen was selected as the reaction coordinate. A sequence of atomic configurations was created by translating the proton in 0.06 Å increments along this axis. When the proton donating species was described by a Zundel cation, the axis connecting the two oxygen atoms was defined as a second reaction coordinate, and the corresponding hydrogen atom was translated along this axis with the same 0.06 Å stride. Two alternate reaction coordinates were considered in the CNT systems: either calculated minimum energy pathways from nudged elastic band[49] simulations were employed directly, or a set of configurations were constructed by translating the transition state configuration along the imaginary vibrational mode corresponding the reaction coordinate.[28] Both of these reaction coordinates involve the movement of several other atoms in addition to the proton that is reduced in the reaction. The impact of using different reaction coordinate representations has been studied in Refs. 50 and 51 in relation to the original SHS model.

The diabatic electronic states defined in Fig. 1b were constructed by imposing suitable charge and magnetization density constraints on the system. For the explicitly solvated carbon nanotube systems, separate constraints were applied to each component involved in the reaction, namely, the reacting proton, the two water molecules that comprise the proton donor, and the electron donating CNT. If the total number of electrons in the system was even, magnetization density constraints were not applied to the diabatic states representing the reactant (IS) and product (FS) states because these constraints were automatically satisfied. Moreover, to maintain net spin parity in such systems, the other diabatic states (ET, HT) were converged to broken symmetry solutions with opposing spin densities on the CNT and proton donor molecular fragments.

The diabatic states at the reaction transition state were solved by using unconstrained DFT densities as the initial guess. Subsequent configurations were restarted from the optimized CDFT solution of the previous configuration along the reaction coordinate, typically reducing the number of CDFT SCF iterations needed to reach convergence to 2-4. For the HBC systems, more approximate constraint definitions were employed to reduce computational cost, because evaluating qualitative trends was our primary objective in these systems. The specifics and an analysis of the effects have been presented in the Supplementary Material.

Throughout this paper, constraint target values are calculated using isolated fragment configurations as reference values, see Sec. II B. A constraint is deemed converged when its value deviates from the target value by at most 10^{-3} electrons. The additive single bond covalent radii[52] for oxygen and hydrogen atoms, and double bond radii[53] for carbon atoms were employed in the construction of the Becke[40] weight functions that define the CDFT constraints. The constraints were optimized using the Newton-Raphson method with backtracking line search and an initial step size $\alpha = 1$. The Jacobian matrix is calculated on each iteration by sequentially perturbing each constraint Lagrangian ξ_j by 5×10^{-3} and minimizing the energy self-consistently.

Electronic structure optimizations used the spin polarized formalism of the Gaussian and planewaves method[44,54] in conjunction with the orbital transformation[42] minimizer. The PBE[55] exchange-correlation functional was adopted for most simulations. Some qualitative tests were conducted with the MPW1K[56] global hybrid functional. The valence electrons of atoms were expanded using molecularly optimized double ζ basis sets,[57] while core electrons were treated with norm conserving pseudopotentials.[58–60] DFT-D3 van der Waals corrections[61] were applied to the PBE simulations. A 500 Ry cutoff was selected for the auxiliary planewave basis in the HBC systems. For consistency with the original study,[28] a higher 550 Ry cutoff and nonlinear core corrected pseudopotentials[62] were employed in the CNT systems. The studied systems were placed in vacuum with at least 10 Å vacuum surrounding the atoms in each direction. Interactions with periodic images were decoupled with a wavelet based Poisson solver.[63] The CNT systems were all charge neutral, while a unit positive charge was applied to the HBC systems.

IV. RESULTS AND DISCUSSION

In order to verify that the CDFT-CI method is suitable for studying the Volmer reaction, benchmark calculations were first conducted using HBC as a model electron donating catalyst. The results for systems with a hydronium cation proton donor in vacuum are reported in Sec. IV A 1, while the effects of solvation are explored Sec. IV A 2 using a Zundel cation proton donor. The method is subsequently applied to HER catalysis on open-ended CNTs. Adiabatic energy profiles for the Volmer reaction are computed with standard DFT and contrasted with CDFT-CI results in Sec. IV B. An extension of the CDFT-CI model to the Heyrovsky reaction step is then presented in Sec. IV C. We conclude with a short discussion on the differences between CDFT-CI and DFT predicted energy profiles and analyze the impact of using different diabatic bases for the CDFT-CI model in Sec. IV D.

A. Volmer reaction on HBC

1. *Hydronium cation in vacuum*

The Volmer reaction model defined in Sec. II A was formulated in terms of four diabatic electronic states, which were depicted in Fig. 1b. The adiabatic Kohn-Sham determinants and the associated ground state energy profile along the Volmer reaction coordinate can be recovered by performing a configuration interaction calculation in the basis of these states. To estimate the importance of each diabatic state in the CI expansion, we will first compare the energy profile obtained with the full set of diabatic states and the results from two alternate two state representations, where only the reactant (IS) and product (FS) states are considered, or the (IS, ET) and (FS, HT) pairs are combined into two effective states via block diagonalization (see Fig. 2). The comparison is carried out by examining the Volmer reaction in a system comprised of a hydronium cation proton donor and a HBC electron donor. The hydronium cation is placed 3.2 Å above the surface, as measured from the oxygen atom, and the reacting proton is translated in 0.06 Å increments along the axis between the oxygen and a carbon atom in the HBC molecule. The adiabatic energy profiles calculated with CDFT-CI using different sets of diabatic states are compared to standard DFT in Fig. 3a.

Examining Fig. 3, it is immediately obvious that CDFT-CI increases the reaction activation energy in comparison to DFT, regardless of the choice of which diabatic states to include in the CI expansion. This result is natural given that the DFT curve was obtained with the PBE functional which is known to suffer from spurious electron delocalization. In addition, we find that CDFT-CI also alters the reaction energy, which in the present case is decreased (more exothermic) in the forward reaction direction. Comparison of the different sets of diabatic states included in the CDFT-CI model shows that the barrier is largest with the two state model, which includes only the IS and FS states, and smallest when all states are included, although the values differ only by 0.06 eV. The barrier obtained with the two effective states constructed by block diagonalization resides in between these two.

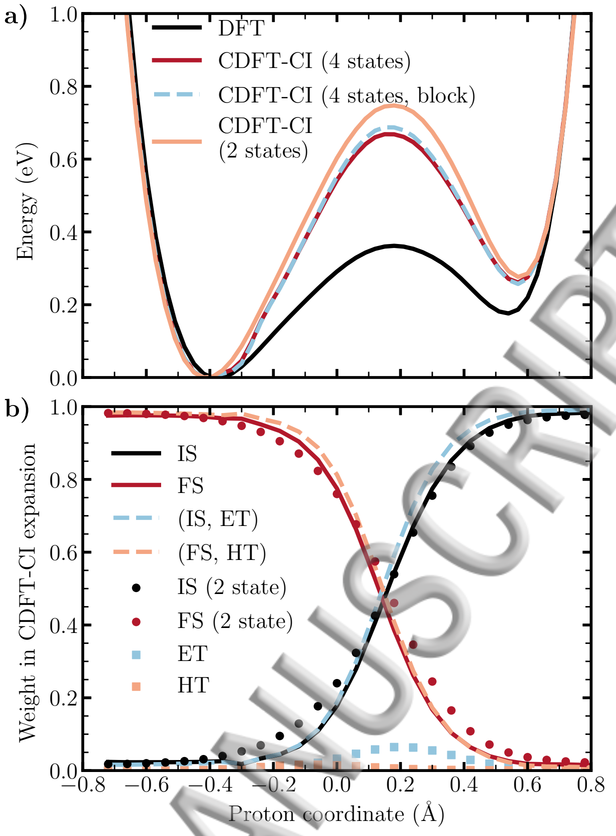

FIG. 3. a) Adiabatic energy profiles calculated with standard DFT and CDFT-CI for the Volmer reaction in the HBC/hydronium system at a fixed 3.2 Å proton acceptor-donor separation. Positive values of the proton coordinate indicate that the proton is closer to the water molecule than to HBC. The CDFT-CI energy profiles are computed using different sets of diabatic states from Fig. 1b in the expansion: full set of four states (denoted 4 states), two effective states obtained by combining (IS, ET) and (FS, HT) pairs with block diagonalization (4 states, block), and only the IS and FS states (2 states). The data has been smoothed using cubic splines. b) Weight of each diabatic state in the CDFT-CI ground state determinants. States in the full four state model are labeled IS, FS, ET and HT, the labels IS (2 state) and FS (2 state) denote states in the model comprised of the reactant and product diabats, while the effective two states in the block diagonalization model are indicated by the (IS, ET) and (FS, HT) labels.

To understand the observed trends in CDFT-CI barrier height, the weight, c_i^2, each diabatic state contributes to the ground state CDFT-CI determinant is plotted against the reaction coordinate in Fig. 3b. This figure demonstrates that the ground state determinant is mostly described by the linear combination of the reactant and product states since their combined weight exceeds ~ 95 % everywhere. However, in the transition state region around 0.2 Å, we observe a small peak (~ 5 %) in the weight of the ET state which can be attributed to the observed reduction in barrier height when the full four state diabatic representation is used. As noted in Sec. II A, the ET state represents a configuration where the electron donating HBC surface has already reduced the reacting proton, but which still is (loosely) bound to the water molecule that originally constituted the hydronium cation. When the off-diagonal states from Fig. 1b are omitted from the CDFT-CI expansion, the transition from the reactant (IS) state to the product (FS) state is more gradual than with the four state model.

The differences between alternate diabatic representations are not limited to ground state properties. Plots similar to those for the ground state in Fig. 3 are shown in Fig. S4 of the Supplementary Material for the first excited state. To summarize, this figure demonstrates that there are significant quantitative and qualitative differences between excited state energy profiles when the size of the CDFT-CI activate space is contracted. As a consequence, large variances are also expected in the predicted values of the electronic coupling V^{el} (see below), which is defined as half of the energy splitting between the ground and first excited state energy profiles at the transition state.[64] The ET diabatic state is again the root cause for the discrepancies between alternate diabatic representations as its weight in the first excited state is over 60 % almost everywhere along the reaction coordinate, which follows naturally from the prior interpretation that the state represents the reduction of the proton. Although alarming at first glance, the stark differences between the effective two state and the full four state CDFT-CI models are fully explained by the properties of the block diagonalization transformation. In particular, despite the inclusion of the ET state in the construction of the block diagonalized basis, it is important to note that the transformation discards almost all information about the excited state behavior because the transformation is a matrix rank reducing operation: only the eigenenergies and eigenstates of the ground block diagonalized state, which is predominantly IS-like at the transition state, are retained in order to reduce the rank of the effective Hamiltonian matrix in half, as shown in Fig. 2.

Because the rate of electron tunneling decays exponentially with distance,[29] the electronic coupling discussed above should exhibit the same decay trend when the proton acceptor-donor distance is increased. To verify that the CDFT-CI method reproduces this result, Volmer reaction energy profiles were generated analogously to Fig. 3 for a total of six proton

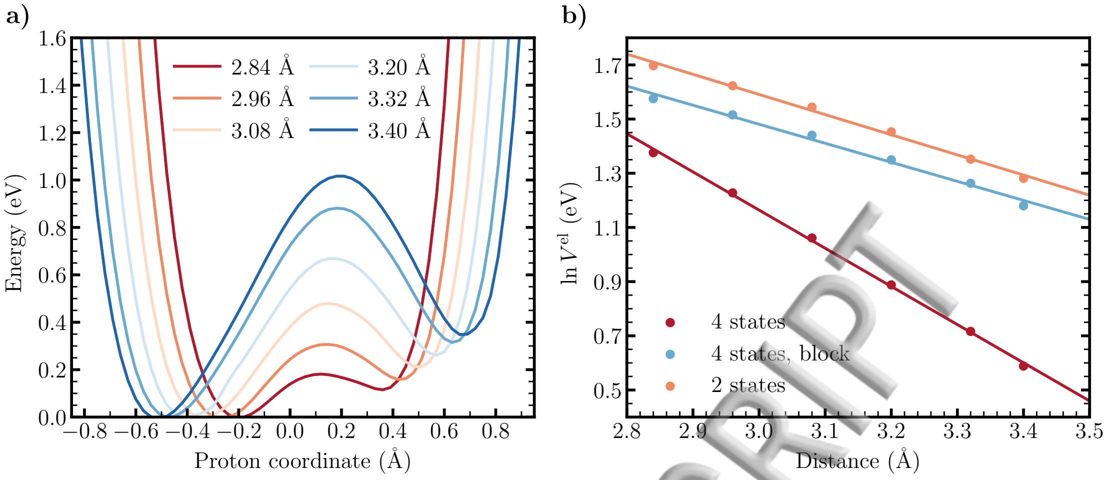

FIG. 4. a) CDFT-CI energy profiles for the Volmer reaction using the full set of four diabatic states in the HBC/hydronium system at various proton acceptor-donor separations. b) Calculated values of the electronic coupling, V^{el}, as a function of the proton acceptor-donor distance. Note the logarithmic scale. The electronic couplings have been evaluated using different diabatic representations, which have been explained in the main text and Fig. 3.

acceptor-donor separations by rigidly translating the hydronium cation. The calculated CDFT-CI energy profiles with the full four state model are shown in Fig. 4a, while values of the electronic coupling computed with all considered diabatic representations are presented in Fig. 4b. Energy profiles obtained with DFT and other considered CDFT-CI models are shown for comparison in Fig. S5 in the Supplementary Material.

The CDFT-CI calculated reaction and activation energies both exhibit an increasing trend when the hydronium cation is translated farther away from the HBC molecule. The observation that the barrier grows as the distance increases is in full accordance with the expected exponential decay of the electron tunneling rate, because the electron has to tunnel through ever greater distances prior to reducing the proton to a hydrogen atom. As shown in Tables S4-S5 in the Supplementary Material, CDFT-CI predicts systematically larger barriers than DFT as the proton acceptor-donor distance is varied. CDFT-CI reaction energies are also more exothermic than DFT but the difference diminishes the greater the separation. Overall, the results are quite insensitive to the employed CDFT-CI diabatic representation: the reaction energies are identical and even the variance in barriers remains within 0.07 eV, which is below the typical 0.1 eV resolution limit attributed to DFT based methods. The trends discussed here for the PBE functional persist when the functional is swapped for the MPW1K global hybrid which includes ∼ 40% exact exchange, see Figs. S6-S8 and Tables S9-S10 in the Supplementary Material.

Fig. 4 also confirms that the correct trend is indeed recovered for the magnitude of the electronic coupling. As noted above, there is a clear difference between alternate diabatic representations stemming from disparities in the first excited CDFT-CI state: the values of the electronic coupling are the smallest with the full four state model and the decay is most pronounced. However, the actual values of the electronic coupling are not that important in the current context because, irrespective of the diabatic representation, the coupling is very large compared to the thermal energy $k_B T$. This implies that the reaction is electronically adiabatic with respect to all nuclear modes and the reaction occurs on the ground electronic state, see below for further analysis.

All in all, the results discussed thus far in this section suggest that ground state properties (activation and reaction energies) are rather insensitive to the choice of diabatic states in the CDFT-CI model, whereas quantitative differences arise in excited state properties if the size of the CI active space is reduced. The preferred safe strategy for applying CDFT-CI to the Volmer reaction, therefore, seems to be to include all diabatic states from Fig. 1b in the model. This conclusion will be reevaluated in Sec. IV D once we have data from further systems (Secs. IV A 2-IV C). First, however, we shall complete the adiabacity analysis started above to verify that the ground state potential energy profile suffices to characterize the Volmer reaction, which will be the primary quantity evaluated in subsequent sections. This analysis involves treating the reacting proton quantum mechanically and subjecting the CDFT-CI model to the same semiclassical treatment which has been adopted with the original SHS model to, e.g., characterize PCET reaction mechanisms.[25,37]

The vibrational wavefunctions that correspond to the reactant (IS) and product (FS) diabatic electronic states as well as to the effective (IS, ET) and (FS, HT) states are depicted in Fig. 5 at a 3.2 Å proton acceptor-donor separation. The vibrational wavefunctions were computed with the Fourier grid Hamiltonian method[32,34] by discretizing the electronic potential energy profiles onto a grid with 1024 points. The ET and HT states modify the reactant and product states surprisingly much when the states are combined into effective states with block diagonalization. This results in a broadening of the proton vibrational wavefunctions, which in turn causes an order of magnitude increase in the value of the

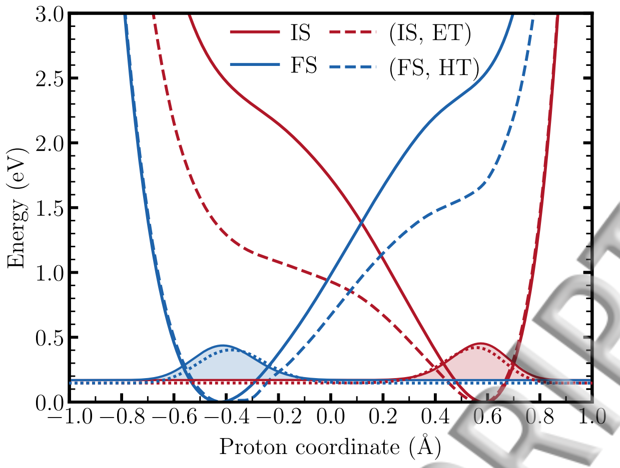

FIG. 5. Energies of the diabatic electronic states as a function of the proton coordinate in the HBC/hydronium system at a 3.2 Å acceptor-donor separation. The solid lines correspond to the IS and FS states, while the dashed lines represent the effective (IS, ET) and (FS, HT) states obtained with block diagonalization. The ground state proton vibrational wavefunctions associated with these electronic states are shown by the filled curves. The minima of the diabatic states are aligned on the energy axis because the vibrational wavefunctions should be degenerate for the semiclassical analysis.

vibrational overlap. These modifications are rationalized by the observation that the energetic separation between the IS (FS) and ET (HT) state pair decreases notably when the hydrogen nucleus is translated away from energy minimum of the IS (FS) diabat.

The values of the semiclassical adiabacity parameter p have been estimated on the basis of the CDFT diabatic states as a function of the proton acceptor-donor separation. The results are tabulated in Tables S6-S8 in the Supplementary Material for all consider diabatic representations. Note that the IS and FS states were employed to compute the vibrational quantities related to the full four state model because the semiclassical analysis is based on a two state formalism. Irrespective of whether the IS and FS or the effective (IS, ET) and (FS, HT) diabatic states are employed in the analysis, the value of adiabacity parameter is large, $p \gg 1$, indicating that the proton tunneling time is significantly slower than the electron transition time, $\tau_\mathrm{p} \gg \tau_\mathrm{e}$. In the context of more general PCET reactions given by Eq. (2), this result could be interpreted as an indication that the reaction proceeds via the hydrogen atom transfer mechanism instead of concerted PCET, i.e., that the proton actually reacts as a neutrally charged hydrogen atom and there is no significant rearrangement of charge density.[25] This mechanism is not directly transferable to the Volmer reaction but it nonetheless offers interesting insight into the reaction. Looking back at Fig. 4, we see that the transition state is attained at a positive value of the proton coordinate, that is, closer to water than to HBC. The FS state becomes the predominant contribution to the CDFT-CI determinant at the same time. Together these observations suggest that the reaction mechanism, very loosely speaking, consists of a fast initial reduction of the proton followed by slower hydrogen transfer. This interpretation is of course an oversimplification because the CDFT-CI wavefunction is multiconfigurational: the system transitions from a predominantly IS-like state to a predominantly FS-like state through a sequence of intermediaries where both states contribute notably. Note that no actual assumptions about the mechanism enter into the CDFT-CI calculation because the weight of each diabat is free to vary according to Eq. (11). The second implication of the result $p \gg 1$ is that the reaction can be fully characterized by the adiabatic ground state potential energy surface (the reaction is both vibronically and electronically adiabatic[65]); however, as the results of this section have shown, standard DFT calculations with GGA functionals might not be reliable in estimating the energy profile.

2. *Zundel cation*

Having verified that the CDFT-CI model is applicable to the Volmer reaction in vacuum, we next validate the proposed strategy for including explicit solvation effects in fragment based CDFT constraints. As described in Sec. II B, the first step of this process is to treat each diabatic electronic state in terms of two separate substates, where either the proton donor (hydronium/Zundel) or acceptor (HBC) is solvated. The substates are next combined into a single effective state with block diagonalization. Here, we will also evaluate the effects of using a different proton donor, namely, the Zundel cation $H_5O_2{}^+$. A second proton coordinate axis is defined between the oxygen atoms of the Zundel cation. Note that the proton/hydrogen moving along this axis is not reduced in the reaction. This two dimensional treatment has been adopted to approximate the concerted motion of the two active hydrogen nuclei participating in the Volmer reaction. The primary reaction coordinate describes the motion of the proton that is reduced in the reaction as it moves from the Zundel cation the HBC surface, while the secondary coordinate models the motion of the hydrogen that is initially delocalized between the Zundel oxygen atoms and becomes fully associated with the proton donating oxygen in the product state. With this scheme, the costly calculation of actual reaction paths can be avoided. Additionally, to estimate the effects of changing Zundel cation oxygen-oxygen separation, the Volmer reaction energy profiles were computed at two Zundel oxygen-oxygen separations, corresponding to the minimum energy configurations of the Zundel cation (2.4 Å) and a water dimer (2.8 Å) in vacuum. A comparison of the vacuum and solvated energy profiles are shown in Fig. 6 for CDFT-CI simulations using the full set of diabatic states.

Focusing first on the effects of explicit solvation, we observe that the water shell stabilizes the reactant state of the reaction, which leads to an increase in the values of the activation and reaction energies when compared to vacuum results, see Tables S11-S12 in the Supplementary Material for the actual quantitative values. The effects are more pronounced for the system where the Zundel oxygen-oxygen distance is set to the shorter value of 2.4 Å. In fact, the reactant state of the other system with the longer O-O distance has two local minima separated by a shallow saddle point. These minima correspond to configurations where both translated hydrogens are either bonded to the same oxygen forming $H_3O_r^+ \cdots H_2O$, or they both are bonded to different oxygens $H_2O_r \cdots H_3O^+$, where O_r denotes the oxygen atom used in defining the primary reaction coordinate with the HBC surface. Neither state truly represents a Zundel cation $H_5O_2^+$, and the actual proton donor in this system is a hydronium cation with the other water molecule acting as an additional solvent molecule.

The addition of solvent causes a similar increasing effect to the value of the electronic coupling calculated at the reaction transition state (Tables S11-S12 in the Supplementary Material), which again is more pronounced for the system with the shorter Zundel O-O separation. In order to estimate whether the choice of diabatic states affects the results, the adiabatic energy profiles from Fig. 6 were reevaluated using the two state CDFT-CI models composed either of the reactant (IS) and product (FS) states or the effective (IS, ET) and (FS, HT) states. The resulting profiles are shown in Figs. S10-S11 of the Supplementary Material, while data for standard DFT with the PBE functional is included for completeness in Fig. S9. The energy parameters from these simulations have also been collected into Tables S11-S12 in the Supplementary Material. Overall, the reaction and activation energies computed with both two state models are in perfect quantitative agreement with the full four

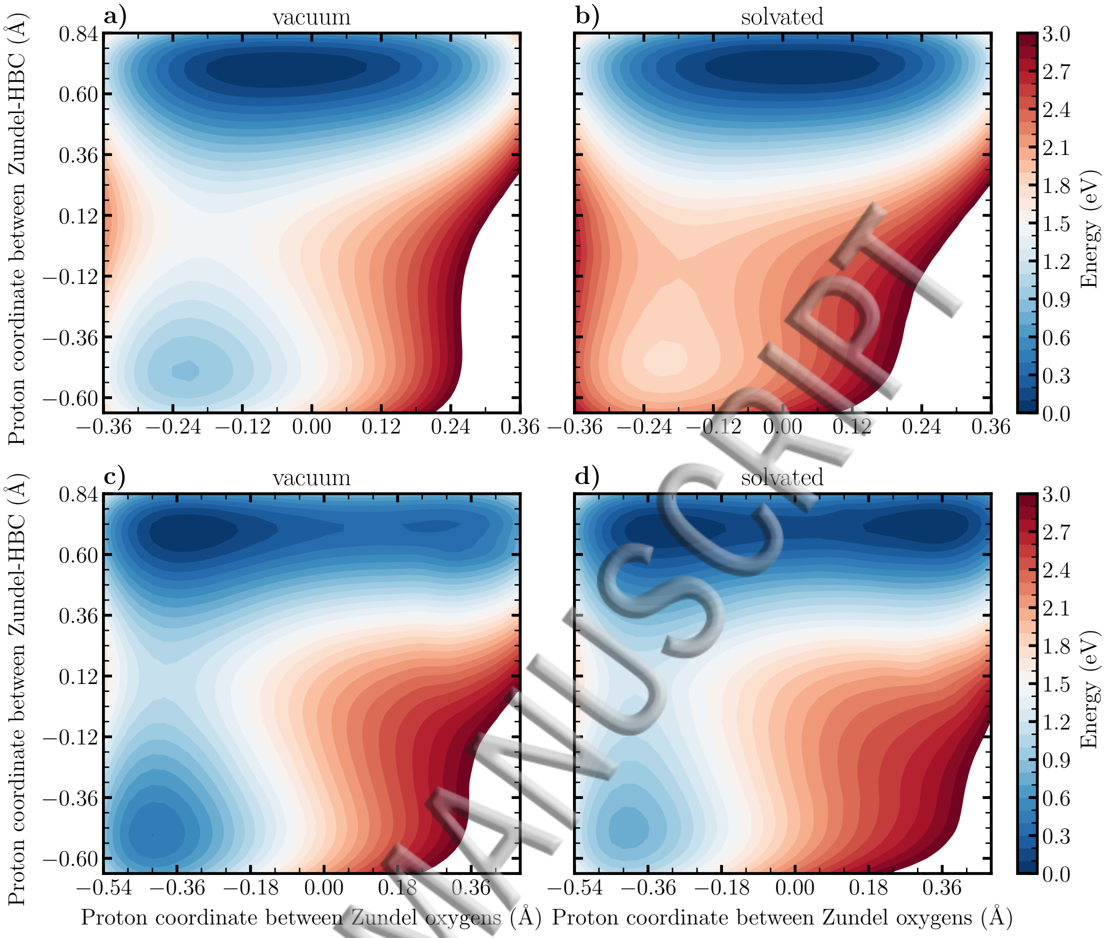

FIG. 6. Two dimensional CDFT-CI energy profiles for the Volmer reaction in the HBC/Zundel system at two Zundel oxygen-oxygen separations, corresponding to the minimum energy configurations of the Zundel [a) – b)] and water dimer [c) – d)] molecules in vacuum. The HBC-Zundel separation is fixed to 3.4 Å in both systems. The vertical reaction coordinate describes the motion of the proton that is reduced to hydrogen in the reaction and binds to HBC in the product state, represented by negative values of the reaction coordinate. The secondary horizontal reaction coordinate describes the motion of the hydrogen atom that is located on the axis connecting the two oxygen atoms of the Zundel cation, with negative values indicating that the atom is closer to the oxygen which donates a proton to HBC. The profiles in [a) & c)] were calculated in vacuum, while explicit solvation was included in the profiles in [b) & d)] by using the block diagonalization strategy described in the main text. The full set of diabatic electronic states from Fig. 1b were included in the CI expansion.

state model. By contrast, standard DFT predicts activation energies 0.1 − 0.3 eV smaller than the CDFT-CI values depending on system, although reaction energies are consistent with the other methods. The values of the electronic coupling exhibit the same increasing trend discussed previously in Sec. IV A 1, growing in order four state model > effective two state model > two state model. The effect of using the MPW1K functional instead of PBE is briefly explored in Sec. S8 in the Supplementary Material.

B. Volmer reaction on CNTs

The previous section IV A demonstrated that the proposed CDFT-CI method can successfully be applied to the Volmer reaction using a simple model system. In this section, we will consider a more complex HER catalyst model by assessing how CDFT-CI influences the catalytic performance of different surface sites at the edge of solvated open-ended carbon nanotubes, which were studied in detail in Ref. 28. Instead of translating the reacting proton along a one dimensional reaction coordinate, we will consider two alternative reaction coordinates where the entire system is translated according to the minimum energy reaction path, obtained via nudged elastic band[49] (NEB) simulations, or where the transition state configuration is translated along the reaction coordinate vibrational mode. CDFT-CI energy profiles were computed for a total of three surface sites using both reaction coordinate representations. The results for two of these sites are compared to standard DFT PBE results in Fig. 7, while data for the remaining site is shown in Fig. S13 of the Supplementary Material. The Zundel cation acts as the proton donating species in each system.

Applying the CDFT-CI model causes substantial modifications of the Volmer energy profiles. The activation energies increase by up to 0.2 eV, while reaction energies in the forward direction decrease by $0.1 - 0.2$ eV, when evaluated on the NEB minimum energy reaction paths. The magnitude of these changes cannot be predicted a priori because CDFT-CI modifies each reaction profile by a different amount. The barriers obtained when the CDFT-CI determinant is expanded in the basis of the effective (IS, ET) and (FS, HT) states are consistently larger than with the full set of four diabats, or with the two state basis comprised of the reactant and product states. The reaction energies, conversely, are identical with all diabatic representations. Although the contribution of the ET and HT states to the four state CDFT-CI vector is small ($< 5 \times 10^{-3}$), combining these together with the reactant and product states yields effective states that are either lower or at most equal

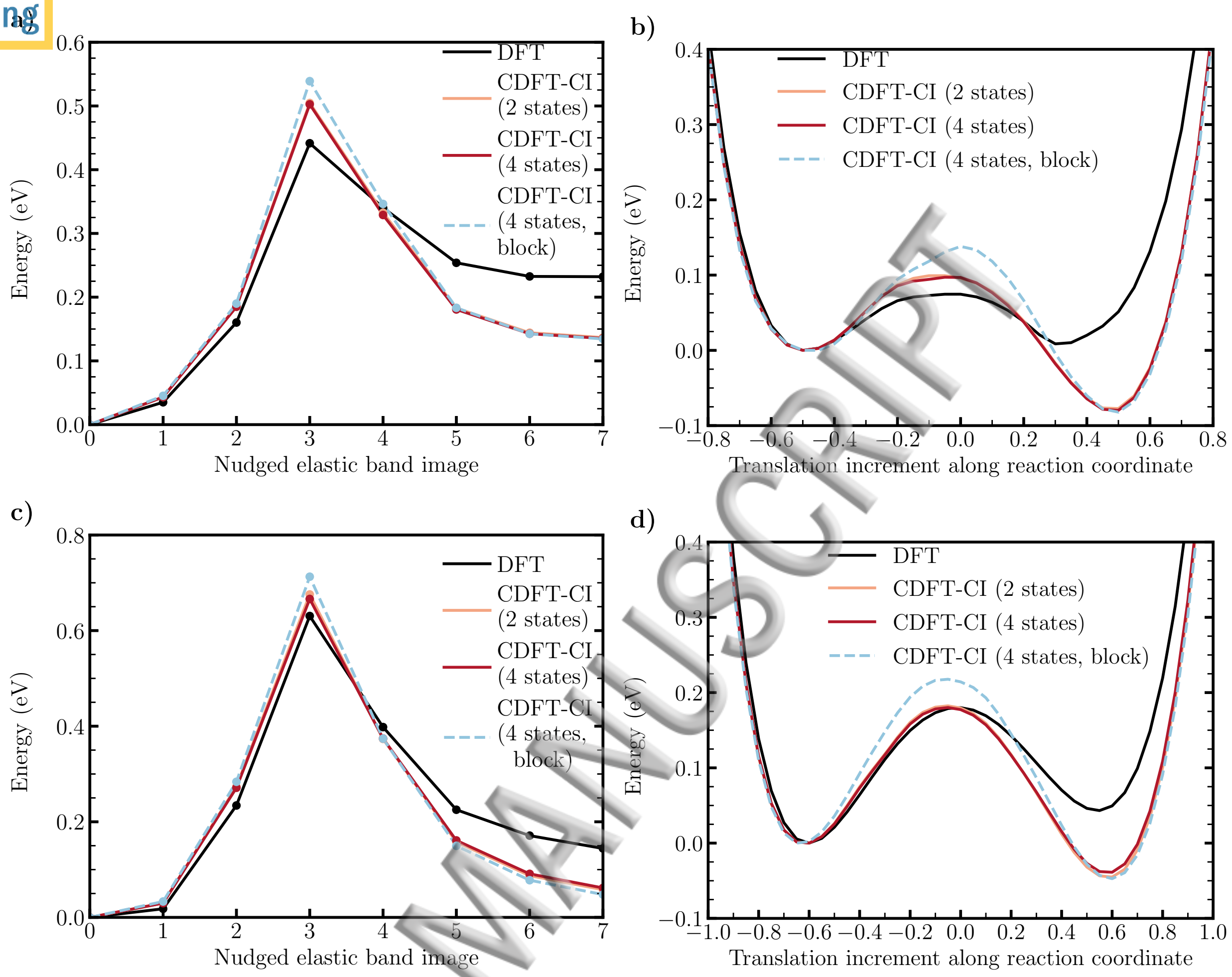

FIG. 7. Comparison of CDFT-CI and DFT PBE energy profiles for the Volmer reaction evaluated at two different surface sites (top/bottom) on the edge of solvated open-ended CNTs taken from Ref. 28. a, c) The system is translated along the minimum energy reaction path obtained from nudged elastic band simulations. b, d) The transition state geometries of these systems, i.e. the highest energy configurations from a) and c), are translated along the reaction coordinate vibrational mode. The CDFT-CI results were computed with three alternate diabatic representations: all four diabatic states from Fig. 1b, the two effective (IS, ET) and (FS, ET) states obtained from the full model by block diagonalization, or the two state model including just the reactant and product states.

in energy to the original IS and FS states, see Fig. S14 in the Supplementary Material. The same figure also reveals that a part of the stabilization arises due to stronger mixing of the IS and ET states around the transition state because the energetic separation between these two states becomes narrower as the system traverses the reaction coordinate. The block diagonalization treatment induces other slight modifications to the diabatic state overlap matrix **S** as well. The joint influence of these factors leads to the observed increase in reaction barriers. The energies of the diabatic states remain relatively unchanged outside the transition state region which explains why the reaction energy predicted by both diabatic representations is equal. The weight of the (effective) initial diabatic state varies between 0.5 to 0.8 depending on system at the transition state, as illustrated in Fig. S14 of the Supplementary Material.

The results discussed above indicate that CDFT-CI stabilizes the product state, where the reduced proton is bound to the active site on the CNT, or, equivalently, destabilizes the initial state configuration in the considered systems. The CDFT constraints were constructed in a manner that prevents any extra charge transfer between the solvent, proton, and the electron and proton donors beyond what is needed to satisfy the constraints. The ambiguity of selecting the ‘correct’ admissible amount of charge transferred was avoided by adopting a fragment based approach (see Sec. II A). Taking all of these notions into account, we can explain the observed results as follows. Firstly, the decrease in the reaction energy suggests that the PBE DFT description of the reactant state deviates more from the CDFT-CI solution than the product state. In the current systems, this manifests as a greater exchange of charge between the electron and proton donors in the reactant state with DFT than with CDFT-CI. Secondly, the increase in the activation energy is a direct result of the enhanced charge localization due to CDFT, consistent with our earlier discussion in Sec. IV A and the findings of Van Voorhis et al.[27] in relation to other chemical reactions.

CDFT-CI also modifies the energy profiles that were constructed by translating the transition state geometry along the reaction coordinate vibrational mode, see Figs. 7b,d. As before, reaction energies in the forward direction are reduced by approximately 0.1 eV. However, the impact on activation energies is not as pronounced: CDFT-CI calculations performed within the basis of the effective block diagonalized states yield systematically larger activation energies than DFT PBE, whereas the full four state and the IS+FS two state models show virtually no difference to DFT PBE in two out of three of the considered systems.

Energy diagrams constructed on the basis of minimum energy reaction paths are a standard tool for comparing the catalytic performance of different surface sites without requiring any input from experimental measurements. In this section, we have shown that CDFT-CI significantly alters the relative stability of the Volmer reaction transition, reactant and product states. As a result, it is obvious that the energy diagrams for the full Volmer-Heyrovsky mechanism will also be modified. The theoretical treatment of the Heyrovsky reaction suffers from the same adverse effects of spurious electron delocalization as the Volmer reaction. We can therefore expect CDFT-CI to influence the energetics of the Heyrovsky reaction as well. To complete our description of the entire reaction mechanism, we will briefly explore how the proposed CDFT-CI model generalizes to the case of the Heyrovsky reaction in the next section.

C. Heyrovsky reaction on CNTs

Generating a set of appropriate diabatic electronic states to represent the Heyrovsky reaction is not as straightforward as for the Volmer reaction, because the reacting proton forms a hydrogen molecule H_2 in the product state instead of binding directly to the electron donating CNT. Moreover, it is not immediately clear how to partition the system into fragment configurations, especially if the two fragment limit on the total number of configurations is maintained. While in principle all possible permutations could be considered, we have opted for a set of diabatic states that are fully analogous to the states employed for the Volmer reaction. To this end, we rewrite the Heyrovsky reaction from Eq. (1) as

$$[(\mathrm{H_2O})_n\text{−}\mathrm{H}]^+ + [\mathrm{H}\text{−}\mathrm{Y}] \rightarrow (\mathrm{H_2O})_n + [\mathrm{H_2}\cdots\mathrm{Y}]^+ \tag{13}$$

In the above expression, the product H_2 molecule has been associated with the electron donating species Y. This choice does not however imply that hydrogen molecule is (covalently) bonded to Y or that it carries any net charge in the product state; on the contrary, it is merely a way to represent the reactant state in the CI expansion. The reaction in Eq. (13) can be represented in terms of four diabatic states that are obtained by performing the appropriate substitutions into Fig. 1b, see Fig. S15 in the Supplementary Material for the resulting states. Solvation effects are included in this model as before by adopting a block diagonalization strategy. The diabatic CDFT states are created by using a total of four charge and four magnetization density constraints, which are applied separately to the CNT, the water molecules that comprise the proton donor, and the two hydrogens that form the hydrogen molecule in the product state (see Sec. III for notes on when the magnetization density constraint can be omitted). CDFT-CI energy profiles were computed for two surface sites using the same reaction coordinate representations considered previously in Sec. IV B. The energy profiles are compared to data obtained with standard DFT and the PBE functional in Fig. 8. The weight each diabat contributes to the CDFT-CI wavefunction has been visualized in Fig. S16 in the Supplementary Material.

The main trends and observations noted for the Volmer reaction in Sec. IV B are preserved when CDFT-CI is applied to the Heyrovsky reaction. Nevertheless, the CDFT-CI treatment appears to have a more profound impact on the energetics of the latter reaction, at least in the absence of additional data. This manifests as a larger overall increase in the values of the activation energies, now ranging between $0.1 - 0.3$ eV. The effect is particularly evident in the values computed by including just the reactant (IS) and product (FS) states or the full set of diabatic electronic states in the CDFT-CI expansion. Interestingly, the barriers with the four state model are slightly lower than with either two state model, whereas they were indistinguishable from the IS+FS two state model in the case of the Volmer reaction. Reaction energies in the forward direction are reduced roughly by a $0.1 - 0.15$ eV constant factor in both systems, in full accordance with the results for the Volmer reaction. Here, the influence of CDFT-CI on reaction energy profiles is quantitatively similar for both of the considered reaction coordinates, contrary to the Volmer reaction case where minimum energy path simulations were more affected.

Although only a limited number of systems were examined in this section, the results have nonetheless demonstrated that the CDFT-CI model that we originally proposed for the Volmer reaction is also suitable to the Heyrovsky reaction, even without extensive modifications of the set of diabatic electronic states included in the model. Summarizing the findings of Sections IV B-IV C, we believe that CDFT-CI could be a powerful tool for generating more accurate energy diagrams for the hydrogen evolution reaction in systems where the reaction proceeds via the Volmer-Heyrovsky mechanism. However, further studies with additional systems and surface sites are necessary to verify these observations. The effects of using a larger set of diabatic states in the CDFT-CI model for the Heyrovsky reaction should be explored as well to ensure model convergence, which was beyond the scope of the current work.

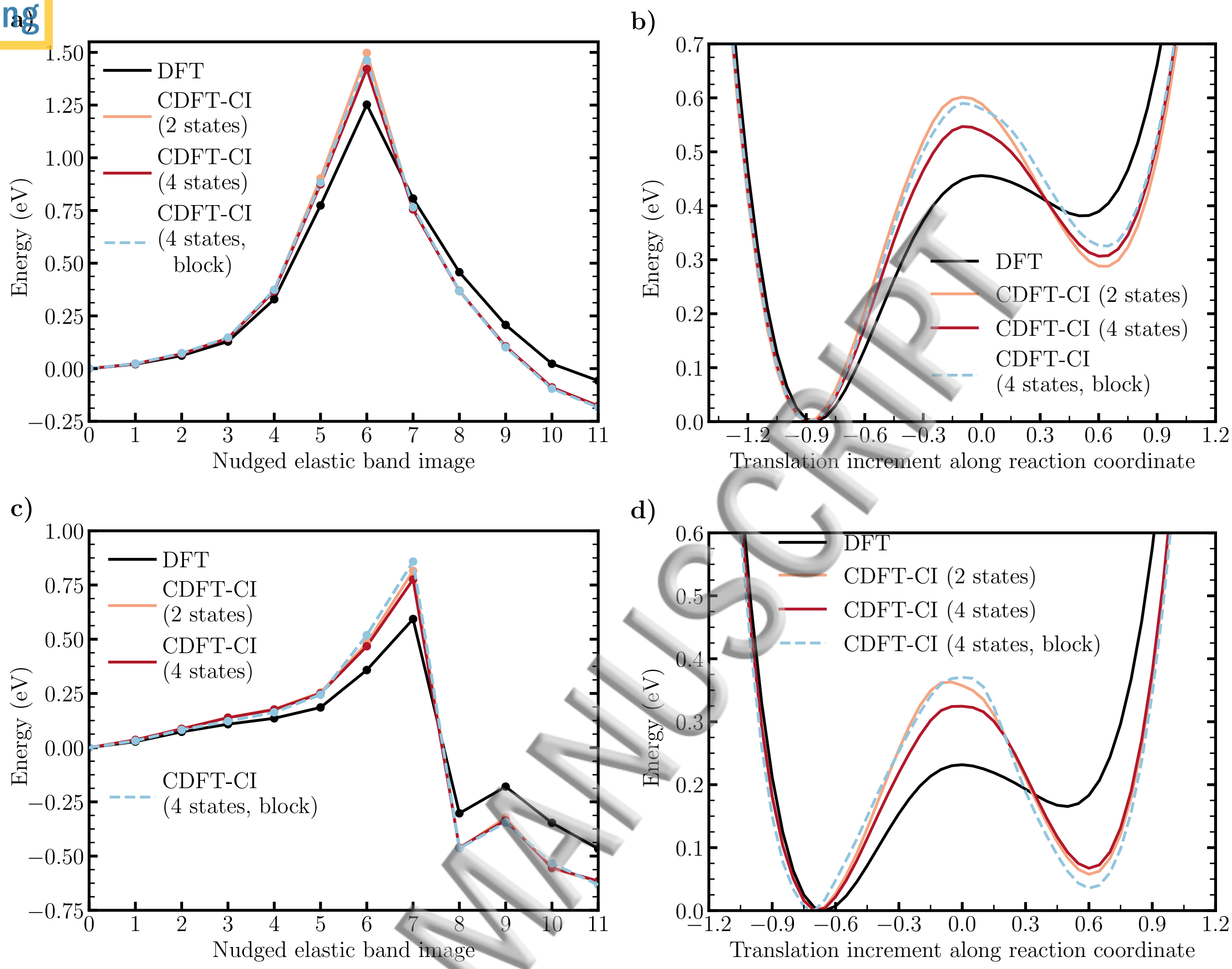

FIG. 8. Comparison of CDFT-CI and DFT PBE energy profiles for the Heyrovsky reaction evaluated at two different surface sites (top/bottom) on solvated open-ended CNTs taken from Ref. 28. a, c) The system is translated along the minimum energy reaction path obtained from nudged elastic band simulations. b, d) The transition state geometries of these systems, i.e. the highest energy configurations from a) and c), are translated along the reaction coordinate vibrational mode. The CDFT-CI results were computed with three alternate diabatic representations: all four diabatic states from Fig. S15 in the Supplementary Material, the two effective (IS, ET) and (FS, ET) states obtained from the full model by block diagonalization, or the two state model including just the reactant and product states.

D. Comparison of DFT and CDFT-CI potential energy surfaces

Sections IV A-IV C have demonstrated a clear difference between DFT and CDFT-CI predicted reaction energy profiles. In CDFT-CI, the adiabatic ground state wavefunction and the associated potential energy surface are created by expanding the wavefunction in terms of charge localized diabatic states. It is therefore not surprising that the disparities between CDFT-CI and DFT arise due to the fact that the charge density is partitioned differently by these two methods. Quantitatively assessing these differences is, unfortunately, limited by the lack of a ground state density for CDFT-CI (only the diabat CI expansion coefficients are available). Instead, to obtain a more qualitative picture of the differences, DFT partial charges are compared to CDFT charges in each diabatic state for a subset of the investigated systems in Figures S17-S22 in the Supplementary Material. The partial charges are plotted separately for each component of the system, i.e., the reacting proton, proton donor, electron donor and solvent.

Examination of the partial charges reveals that DFT charges not only differ from CDFT values in the transition state region but also in the reactant and product reaction states, where the CDFT-CI state is almost fully described by either the IS or FS state, respectively. Significant differences of DFT partial charges to the latter two reaction states correlate with the observed reduction of reaction energies in these systems. Moreover, the figures suggest that according to CDFT-CI the electron donor HBC/CNT loses more charge density than predicted by DFT during the course of the reaction, reaching roughly 0.2 e in the CNT systems if we assume that the IS and FS states fully determine the multireference reactant and product states, respectively. Large variances in CDFT and DFT charges are evident in the transition states of each system. Because multiple diabats contribute to the CDFT-CI transition state, establishing a direct relationship between these differences and the increased barrier is however not possible. As a reminder, the constraint target charges for CDFT were obtained through a fragment constraint approach by splitting the system into appropriate isolated components, see Sec. II B for additional details. This methodology has been shown to be a reliable way of partioning charge density in strongly interaction systems, but it is not entirely immune to exchange-correlation functional effects particularly with complex fragments, e.g., explicitly solvated, elongated Zundel cation.[27,41]

In this work, the CDFT-CI potential energy surfaces were evaluated by considering three alternate diabatic representations on the basis of Fig. 1b and Fig. S15 in the Supplementary Material. The diabatic states corresponding to the reactant (IS) and product (FS) configurations of the investigated reactions are by far the most important contributions to the CDFT-CI wavefunction, as evident by their combined weight to full four state model that exceeds 95 % everywhere along the reaction coordinate in all systems. Qualitatively, all diabatic representations produced consistent trends in comparison to DFT, namely, increased barriers, and unchanged or reduced reaction energies depending on system. Minor system specific quantitative differences were however observed, although they remain below 0.1 eV in each case. Whenever discrepancies between activation energies were noted, the four state model always predicted the smallest values while the ordering of the two state models varied. Reaction energies were less affected and exhibited no obvious trend, mainly manifesting in a subset of the studied Heyrovsky reactions, see Fig. 8 panels b and d. These observations reflect the significant weight of the IS and FS states; larger differences between diabatic representations are likely to arise in systems where the contribution of the off-diagonal states is more pronounced. By contrast, excited state properties indicated a stronger dependence on the diabatic basis stemming from disparities in the first excited state induced by the reduction of the CI active space, although these differences had no bearing on the main conclusions regarding electronic adiabacity. The impact of the additional block diagonalization step that transforms the four state model into an effective two state model is difficult to analyze in detail because the repeated diagonalizations and rotations modify the relevant CDFT-CI interaction matrices ($\mathbf{H}$, $\mathbf{S}$) in a nontrivial manner: the transformation not only induces subtle changes to the overall contribution of each diabat but also discards some information as the result of the matrix rank reduction, see Sec. II B for details.

Based on the data in Secs. IV A-IV C, it remains unclear when it is sufficient to use just the reactant and product states in CDFT-CI and when additional diabats are required. The use of only two states without loss of accuracy would naturally be preferable owing to the reduced computational effort. Decidedly, the issue of which diabatic representation to employ warrants further investigation. Future studies might benefit from the development of a tool to directly compare the electronic properties of CDFT-CI and DFT wavefunctions. Construction of a high quality reference database for the Volmer-Heyrovsky mechanism would obviously aid in this matter and also enable the systematic testing of exchange-correlation functionals, which was beyond the scope of the current manuscript where an emphasis was placed on typical system sizes found in surface electrocatalysis applications. Another research direction that might further elucidate the properties of the CDFT-CI wavefunction could be to compare the method to block-localized DFT based CI,[66,67] where valence bond type diabatic states are constructed directly in terms of localized orbitals.

V. CONCLUSIONS

In computational electrochemistry, the electrocatalytic performance of catalyst materials is often measured by constructing energy diagrams on the basis of minimum energy reaction paths, which are calculated for the elementary steps that comprise a reaction. The relative stability of configurations along DFT simulated reaction paths suffer from spurious electron delocalization effects, which leads to inaccuracies in the estimated values of reaction and activation energies.

In this paper, we proposed a constrained DFT model for alleviating the effects of spurious electron delocalization in the simulation of the Volmer-Heyrovsky mechanism of the hydrogen evolution reaction, building upon the general treatment of proton-coupled electron transfer reactions by Soudackov and Hammes-Schiffer.[23–25] This model involves representing atomic configurations sampled along the reaction coordinate in terms of a set of diabatic electronic states constructed by imposing suitable density constraints. The diabatic states correspond to the reactant and product states of the reaction as well as two intermediate states where electron transfer either proceeds or follows hydrogen transfer. Refined adiabatic minimum energy reaction profiles are subsequently recovered by performing a configuration interaction calculation in the basis of the CDFT diabatic states.

The CDFT-CI method was first extensively benchmarked by investigating the effects of explicit solvation and using different proton donors for the Volmer reaction with a simple model catalyst. We then examined the full Volmer-Heyrovsky reaction mechanism in open-ended carbon nanotube systems originally characterized in Ref. 28. These simulations demonstrated that CDFT-CI alters the relative stability of the reaction transition, product and reactant states, which lead to an increase in activation energies and a decrease in reaction energies in the examined systems. Reduced electron delocalization and the prevention of excessive charge transfer between different components of the system were deemed to be the main causes for the observed trends.

The proposed CDFT-CI approach is an a posteriori correction method. It thus offers a relatively cheap way for improving DFT calculated energy diagrams by considering only the relevant reaction states. In principle, the reaction minimum energy paths could also be optimized directly at the CDFT-CI level if the necessary nuclear gradients were implemented, which might lead to further accuracy improvements.[68] Given the success we observed in generalizing the model from the Volmer to the Heyrovsky reaction, we expect similar CDFT-CI models with suitably selected diabatic electronic states to be applicable to other electrocatalytically interesting PCET reactions as well, e.g., to the oxygen reduction reaction.

SUPPLEMENTARY MATERIAL

See supplementary material for method validation calculations, further computational details, and additional results related to the systems discussed in Secs. IV A-IV D presented as tables and figures.

ACKNOWLEDGMENTS

This study was funded by the Academy of Finland through its Centres of Excellence program, project no. 251748. N.H. is supported by Aalto University School of Chemical Engineering through a PhD scholarship. Computational resources were provided by CSC–IT Center for Science, Finland.

REFERENCES

[1] Y. Zheng, Y. Jiao, M. Jaroniec, and S. Z. Qiao, Angew. Chem. Int. Ed. **54**, 52 (2015).

[2] Z. W. Seh, J. Kibsgaard, C. F. Dickens, I. Chorkendorff, J. K. Nørskov, and T. F. Jaramillo, Science **355**, eaad4998 (2017).

[3] K. S. Exner, I. Sohrabnejad-Eskan, and H. Over, ACS Catal. **8**, 1864 (2018).

[4] J. K. Nørskov, T. Bligaard, J. Rossmeisl, and C. H. Christensen, Nat. Chem. **1**, 37 (2009).

[5] S. Curtarolo, G. L. Hart, M. B. Nardelli, N. Mingo, S. Sanvito, and O. Levy, Nat. Mater. **12**, 191 (2013).

[6] Y. Jiao, Y. Zheng, M. Jaroniec, and S. Z. Qiao, Chem. Soc. Rev. **44**, 2060 (2015).

[7] E. Skúlason, V. Tripkovic, M. E. Björketun, S. Gudmundsdóttir, G. Karlberg, J. Rossmeisl, T. Bligaard, H. Jónsson, and J. K. Nørskov, J. Phys. Chem. C **114**, 18182 (2010).

[8] W. Gao, J. A. Keith, J. Anton, and T. Jacob, J. Am. Chem. Soc. **132**, 18377 (2010).

[9] Y.-H. Fang and Z.-P. Liu, J. Am. Chem. Soc. **132**, 18214 (2010).

[10] C. P. Plaisance and R. A. van Santen, J. Am. Chem. Soc. **137**, 14660 (2015).

[11]H. A. Hansen, V. Viswanathan, and J. K. Nørskov, J. Phys. Chem. C **118**, 6706 (2014).

[12]R. Jinnouchi and R. Asahi, J. Phys. Chem. Lett. **8**, 4279 (2017).

[13]X. Ma, Z. Li, L. E. K. Achenie, and H. Xin, J. Phys. Chem. Lett. **6**, 3528 (2015).

[14]R. Gasper, H. Shi, and A. Ramasubramaniam, J. Phys. Chem. C **121**, 5612 (2017).

[15]Y. Xu, M. Kraft, and R. Xu, Chem. Soc. Rev. **45**, 3039 (2016).

[16]K. Chan and J. K. Nørskov, J. Phys. Chem. Lett. **7**, 1686 (2016).

[17]S. Sakong and A. Groß, ACS Catal. **6**, 5575 (2016).

[18]R. Jinnouchi, K. Kodama, and Y. Morimoto, Curr. Opin. Electrochem. (2018), https://doi.org/10.1016/j.coelec.2018.03.024.

[19]A. J. Cohen, P. Mori-Sánchez, and W. Yang, Chem. Rev. **112**, 289 (2012).

[20]Q. Wu and T. Van Voorhis, Phys. Rev. A **72**, 024502 (2005).

[21]Q. Wu and T. Van Voorhis, J. Chem. Theory Comput. **2**, 765 (2006).

[22]B. Kaduk, T. Kowalczyk, and T. Van Voorhis, Chem. Rev. **112**, 321 (2012).

[23]A. Soudackov and S. Hammes-Schiffer, J. Chem. Phys. **111**, 4672 (1999).

[24]S. Hammes-Schiffer and A. V. Soudackov, J. Phys. Chem. B **112**, 14108 (2008).

[25]S. Hammes-Schiffer and A. A. Stuchebrukhov, Chem. Rev. **110**, 6939 (2010).

[26]Q. Wu, C.-L. Cheng, and T. Van Voorhis, J. Chem. Phys. **127**, 164119 (2007).

[27]Q. Wu, B. Kaduk, and T. Van Voorhis, J. Chem. Phys **130**, 034109 (2009).

[28]N. Holmberg and K. Laasonen, J. Phys. Chem. Lett. **6**, 3956 (2015).

[29]J. Blumberger, Chem. Rev. **115**, 11191 (2015).

[30]A. Migliore, N. F. Polizzi, M. J. Therien, and D. N. Beratan, Chem. Rev. **114**, 3381 (2014).

[31]A. V. Soudackov and S. Hammes-Schiffer, Chem. Phys. Lett. **299**, 503 (1999).

[32]C. C. Marston and G. G. Balint-Kurti, J. Chem. Phys. **91**, 3571 (1989).

[33]K. Drukker and S. Hammes-Schiffer, J. Chem. Phys. **107**, 363 (1997).

[34]S. P. Webb and S. Hammes-Schiffer, J. Chem. Phys. **113**, 5214 (2000).

[35]A. V. Barzykin, P. A. Frantsuzov, K. Seki, and M. Tachiya, "Solvent effects in nonadiabatic electron-transfer reactions: Theoretical aspects," in *Advances in Chemical Physics* (Wiley-Blackwell, 2003) Chap. 9, pp. 511–616.

[36]A. Soudackov and S. Hammes-Schiffer, J. Chem. Phys. **113**, 2385 (2000).

[37]Y. Georgievskii and A. A. Stuchebrukhov, J. Chem. Phys. **113**, 10438 (2000).

[38]J. E. Subotnik, J. Vura-Weis, A. J. Sodt, and M. A. Ratner, J. Phys. Chem. A **114**, 8665 (2010).

[39]N. Holmberg and K. Laasonen, J. Chem. Theory Comput. **13**, 587 (2017).

[40]A. D. Becke, J. Chem. Phys. **88**, 2547 (1988).

[41]J. Řezáč and A. de la Lande, J. Chem. Theory Comput. **11**, 528 (2015).

[42]J. VandeVondele and J. Hutter, J. Chem. Phys. **118**, 4365 (2003).

[43]D. D. O'Regan and G. Teobaldi, Phys. Rev. B **94**, 035159 (2016).

[44]J. VandeVondele, M. Krack, F. Mohamed, M. Parrinello, T. Chassaing, and J. Hutter, Comput. Phys. Commun. **167**, 103 (2005).

[45]J. Hutter, M. Iannuzzi, F. Schiffmann, and J. VandeVondele, Wiley Interdiscip. Rev.: Comput. Mol. Sci. **4**, 15 (2014).

[46]A. Sirjoosingh and S. Hammes-Schiffer, J. Phys. Chem. A **115**, 2367 (2011).

[47]A. V. Soudackov and S. Hammes-Schiffer, J. Phys. Chem. Lett. **5**, 3274 (2014).

[48]A. K. Harshan, T. Yu, A. V. Soudackov, and S. Hammes-Schiffer, J. Am. Chem. Soc. **137**, 13545 (2015).

[49]G. Henkelman, B. P. Uberuaga, and H. Jónsson, J. Chem. Phys. **113**, 9901 (2000).

[50]A. Sirjoosingh and S. Hammes-Schiffer, J. Chem. Theory Comput. **7**, 2831 (2011).

[51]B. Auer, L. E. Fernandez, and S. Hammes-Schiffer, J. Am. Chem. Soc. **133**, 8282 (2011).

[52]P. Pyykkö and M. Atsumi, Chem. Eur. J. **15**, 186 (2009).

[53]P. Pyykkö and M. Atsumi, Chem. Eur. J. **15**, 12770 (2009).

[54]G. Lippert, J. Hutter, and M. Parrinello, Mol. Phys. **92**, 477 (1997).

[55]J. P. Perdew, K. Burke, and M. Ernzerhof, Phys. Rev. Lett. **77**, 3865 (1996).

[56]B. J. Lynch, P. L. Fast, M. Harris, and D. G. Truhlar, J. Phys. Chem. A **104**, 4811 (2000).

[57]J. VandeVondele and J. Hutter, J. Chem. Phys. **127**, 114105 (2007).

[58]S. Goedecker, M. Teter, and J. Hutter, Phys. Rev. B **54**, 1703 (1996).

[59]C. Hartwigsen, S. Goedecker, and J. Hutter, Phys. Rev. B **58**, 3641 (1998).

[60]M. Krack, Theor. Chem. Acc. **114**, 145 (2005).

[61]S. Grimme, J. Antony, S. Ehrlich, and H. Krieg, J. Chem. Phys.. **132**, 154104 (2010).

[62]A. Willand, Y. O. Kvashnin, L. Genovese, Á. Vázquez-Mayagoitia, A. K. Deb, A. Sadeghi, T. Deutsch, and S. Goedecker, J. Chem. Phys. **138**, 104109 (2013).

[63]L. Genovese, T. Deutsch, A. Neelov, S. Goedecker, and G. Beylkin, J. Chem. Phys. **125**, 074105 (2006).

[64] A. Migliore, J. Chem. Theory Comput. **7**, 1712 (2011).

[65] S. Hammes-Schiffer, Energy Environ. Sci. **5**, 7696 (2012).

[66] A. Cembran, L. Song, Y. Mo, and J. Gao, J. Chem. Theory Comput. **5**, 2702 (2009).

[67] A. Grofe, Z. Qu, D. G. Truhlar, H. Li, and J. Gao, J. Chem. Theory Comput. **13**, 1176 (2017).

[68] B. Kaduk, T. Tsuchimochi, and T. Van Voorhis, J. Chem. Phys. **140**, 18A503 (2014).